

Effect of ZSM-5 Zeolite Morphology on Catalytic Performance of Benzene-ethanol Alkylation

ZHANG Liang, XIA Fei, YUAN Ya-fei, LI Xiao-xian, GUO Shu-jing, ZHANG Wei*

(Dalian Institute of Chemical Physics Xi'an Clean Energy (Chemical Industry) Research Institute, Shaanxi Yanchang Petroleum (Group) Co., Ltd., Xi'an 710065, China)

Abstract: In this paper, four kinds of nano-ZSM-5 zeolites with different morphologies and sizes, including cyclic, lamelliform, spheroidal aggregates, and small particles, were prepared by hydrothermal methods. The synthesized zeolites were characterized by X-ray diffraction (XRD), scanning electron microscope (SEM), Brauer-emmett-teller (BET), solid state nuclear magnetic resonance (MAS-NMR) and ammonia temperature programmed desorption (NH₃-TPD), and the effects of the morphology on the alkylation properties of benzene and ethanol were investigated. The experimental results showed that zeolites with different morphologies had similar weak acid peak strengths at the similar Si/Al ratio. The presence of short B-axes and hollow structures reduces the strength of the strong acid peak in zeolite, which directly affects the alkylation performance. The catalytic alkylation performance of the four zeolite forms decreased in the order of lamellar ZSM-5, cyclic ZSM-5, spheroidal aggregates ZSM-5, and small particle ZSM-5. Under the conditions of lower acid strength, larger specific surface area and pore volume, and more straight pores, the best alkylation performance of zeolite and the greater selectivity of ethylbenzene were achieved.

Key words: ZSM-5 zeolite; synthesis; morphology; catalytic performance

CLC number: O643.32

Document code: A

DOI: 10.16084/j.issn1001-3555.2024.03.001

Ethylbenzene is an important basic organic monomer raw material in the chemical industry^[1]. Ethylbenzene is mainly used for catalytic dehydrogenation to produce styrene, which accounts for more than 90% of the total styrene production capacity. A small amount of ethylbenzene is used as a solvent or for dilution and organic synthesis, such as in the production of diethylbenzene. Styrene is an important monomer of high-molecular-weight polymers^[2], and the market demand for styrene has shown an increasing trend annually, which directly drives the production of ethylbenzene. At present, ethylbenzene is mainly prepared by ethylene and benzene alkylation, including pure ethylene and dilute ethylene (dry gas) as the raw material. The latter is a mature process mainly used in current industry, among which the SGEb (dry gas phase ethylbenzene production process) independently developed by Sinopec is the most typical^[3]. Ethylene has been widely used as an alkylating agent, but the uneven distribution of ethylene resources makes it difficult to effectively promote or implement in areas lacking ethylene resources^[4-5]. As a compensation resource, ethanol is a highly active alkylating agent with a wide range of sources. Traditional ethanol mainly comes from grain fermentation, and the successful production of domestic coal-based ethanol products and the important progress in bioethanol technology provided additional possibilities for the further utilization of ethanol. The method of producing ethylbenzene by the reaction of ethanol with benzene has been widely studied^[6-8]. One-step

gas-phase synthesis of ethylbenzene from ethanol and benzene reduces the investment and operation costs of ethanol dehydration equipment. In addition, ethanol, as an alkylating agent, is relatively simple to use in terms of raw material transportation and convenient storage, which provides a new route for ethylbenzene synthesis in areas with excess ethanol capacity and a lack of ethylene resources.

The alkylation of benzene and ethanol follows the mechanism of a positive carbon ion reaction^[9], and zeolite catalysts (such as ZSM-5, β , Y, and MCM-22 zeolites) are generally used in related research^[10-14]. Among them, the ZSM-5 zeolite has been studied the most and has attracted the most attention. The alkylation performance of benzene and ethanol is affected by many factors, such as reaction temperature, the benzene-alcohol ratio of the raw material, space velocity, and pressure, among which the acidity of the ZSM-5 catalyst plays a decisive role. Studies have shown that the side reactions of alkylation reactions, such as the cleavage, disproportionation, and isomerization reactions of ethylbenzene and polyalkylbenzene, occur mainly at the strong acid sites of catalysts, while lower numbers of strong acid sites and higher B-acid density are conducive to improving the selectivity of ethylbenzene^[15]. Zhang *et al.*^[15] reported that selective dealumination or the introduction of P effectively reduced the strong acidity of ZSM-5 zeolite and improved the selectivity of ethylbenzene. Moreover, P also improved the hydrothermal stability of the

Received date: 2024-02-29; **Revised date:** 2024-04-02.

Foundation: Key Research and Development Plan of Shaanxi Province (2023-YBGY-290) and Research Project of Shaanxi Yanchang Petroleum (Group) Co., Ltd. (No. ycsy2023ky-B-81).

Biography: Zhang Liang(1991-), male, master, engineer, mainly engaged in research of benzene-ethanol alkylation. E-mail: LiangZ_6688@163.com, Tel: 029-89853923.

* Corresponding authors. E-mail: ycsy_zw@163.com, Tel: 029-88899565.

molecular sieve and increased the life of the catalyst. The ZSM-5 zeolite has two pore structures, straight and sinusoidal. Through molecular dynamics simulations of the alkylation reaction between benzene and methanol^[16], small molecules tend to diffuse along straight and Z-shaped pore channels, while benzene and alkyl benzene diffuse only along straight pore channels. In addition, the anisotropic length of ZSM-5 zeolite affects the conversion, selectivity, and stability of the catalytic reaction, and differences in synthesis conditions affect the characteristics of the molecular sieve itself, such as zeolite structure and acidity. Huang *et al.*^[17] investigated the catalytic performance of ZSM-5 zeolites with different morphologies and reported that nanosheet or nanospheroidal ZSM-5 zeolites with larger specific surface areas had greater gasoline selectivity and significantly improved one-way life. Zheng *et al.*^[18] described the preparation of multistage porous ZSM-5 molecular sieve and its application in the alkylation reaction of benzene and ethylene in oil refining in detail. Li *et al.*^[19] introduced the research progress of catalysts for benzene and methanol alkylation from Si/Al, crystal size and modification of ZSM-5. Similarly, Zhu *et al.*^[20] demonstrated that ZSM-5 with a short b-axis (thickness of 90 nm) exhibited better catalytic performance than traditional ZSM-5 in the alkylation of benzene with ethanol, which was attributed to its short diffusion path and optimized acidity.

During the alkylation of benzene and ethanol, the distribution of acid sites affects the catalytic performance. Our previous study revealed^[21] that the existence of annular ZSM-5 zeolite hollow structures changed the distribution of B and L acids in molecular sieves, thus affecting the selectivity of ethylbenzene. In addition to the above influencing factors, the diffusion behavior of raw materials and products also significantly affects the activity, selectivity, and catalyst stability of the reaction.

Based on the above analysis, four kinds of ZSM-5 zeolites with the same Si-Al ratio, similar acidity, and different morphologies and sizes were synthesized for the alkylation of benzene and ethanol by the conventional hydrothermal synthesis method, including ring ZSM-5 zeolites, nano-sheet ZSM-5, nanoaggregate-spheroids, and small-grain ZSM-5 zeolites. The effects of the morphology and size of ZSM-5 zeolites on the alkylation of benzene-ethanol were evaluated from the perspectives of product diffusion and the pore structure of the molecular sieve.

1 Experimental

1.1 Experimental materials

Tetraethyl orthosilicate (TEOS, 98%) was provided by Tianjin Kemiou Chemical Reagent Co., Ltd. Sodium meta-aluminate (NaAlO_2) was supplied by Shanghai Titan Technology Co., Ltd. Tetrapropyl ammonium hydroxide (TPAOH, 25%) was obtained from Zhejiang Kent Chemical Co., Ltd. Sodium hydroxide (NaOH), ammonium chloride (NH_4Cl), benzene (C_6H_6), ethanol ($\text{C}_2\text{H}_5\text{OH}$), and sodium chloride (NaCl) were purchased from Shanghai Titan Technology Co., Ltd. Deionized water was made in the laboratory.

1.2 Preparation of zeolites

Preparation of cyclic ZSM-5 zeolites: Annular hollow ZSM-5 zeolite powder with $n(\text{SiO}_2) : n(\text{Al}_2\text{O}_3) = 60$ was synthesized according to the methods described in the literature [21]. NaOH and NaAlO_2 of a certain mass were weighed at

room temperature, an appropriate amount of deionized water and TPAOH were added, and the mixture was fully stirred until completely dissolved. During the process of drip and stir, TEOS was added to the precursor solution in batches at a low temperature ($0\text{ }^\circ\text{C}$). After dropping and stirring at a low temperature for 4 h, a white gel molecular sieve crystallization initial gel was obtained. The molar ratio of the raw material in the gel solution was $10\text{ TPAOH} : 30\text{ SiO}_2 : 0.5\text{ Al}_2\text{O}_3 : 1\text{ 000 H}_2\text{O} : 2\text{ NaOH}$. The initial crystallization liquid was transferred to a hydrothermal synthesis reactor and fixed in a homogeneous reactor, and the crystallization product was obtained by dynamic rotation at $30\text{ r}\cdot\text{min}^{-1}$ at $170\text{ }^\circ\text{C}$ for 24 h. The crystallization products were subsequently washed in deionized water to neutral and dried in a drying oven at $110\text{ }^\circ\text{C}$ for 8 h. A Cyclic ZSM-5 zeolite was obtained by calcining at $550\text{ }^\circ\text{C}$ for 6 h, denoted as C-Z5.

Preparation of lamelliform ZSM-5 zeolites: According to the method^[20], a thin-sheet ZSM-5 zeolite with $n(\text{SiO}_2) : n(\text{Al}_2\text{O}_3) = 60$ was synthesized, and the molar composition of the initial gel was $5.4\text{ TPAOH} : 30\text{ SiO}_2 : 0.5\text{ Al}_2\text{O}_3 : 800\text{ C}_2\text{H}_5\text{OH} : 1\text{ 340 H}_2\text{O} : 1\text{ NaOH}$. The initial gel preparation process was as follows: a molar ratio of NaAlO_2 , NaOH, TPAOH, and $\text{C}_2\text{H}_5\text{OH}$ was weighed and mixed with deionized water and stirred at room temperature for 1 h until the cloudy solution became clear. Then, TEOS was slowly added to the solution, and the precursor gel was obtained after aging at room temperature for 4 h. Finally, the precursor gel was transferred to a hydrothermal synthesis vessel and crystallized at $170\text{ }^\circ\text{C}$ for 24 h, after which the crystallization product was obtained. The product was centrifuged, washed with deionized water to a neutral pH, transferred to a drying oven, dried at $80\text{ }^\circ\text{C}$ for 8 h, and then roasted at $550\text{ }^\circ\text{C}$ for 6 h, the lamelliform ZSM-5 zeolites (L-Z5) were obtained.

Preparation of spheroidal nano-aggregates ZSM-5 zeolites: According to the methods mentioned in the literature [22], multistage porous ZSM-5 zeolites with $n(\text{SiO}_2) : n(\text{Al}_2\text{O}_3) = 60$ were synthesized. The molar composition of the initial gel was $5\text{ TPAOH} : 60\text{ SiO}_2 : 1\text{ Al}_2\text{O}_3 : 10\text{ Na}_2\text{O} : 7\text{ 856 H}_2\text{O}$. The preparation process of the initial gel was as follows: A certain molar ratio of TPAOH, NaAlO_2 , and deionized water was mixed until the clear liquid was clear, TEOS was added dropwise, and the precursor gel was obtained by stirring for 0.5 h. The precursor gel solution was aged at $100\text{ }^\circ\text{C}$ for 3 h and then transferred to a high-pressure synthesis reactor for crystallization at $180\text{ }^\circ\text{C}$ for 3 h. The crystallization products were obtained. The crystallization products were washed with deionized water to a neutral pH, dried in a drying oven at $110\text{ }^\circ\text{C}$ for 8 h, and calcined at $550\text{ }^\circ\text{C}$ for 6 h to obtain spheroidal nanoaggregate ZSM-5 zeolites (N-Z5).

Preparation of conventional small-grain ZSM-5 zeolites: The preparation method of conventional small-grain zeolites is the same as that in the literature [21]. However, TEOS was added at room temperature to obtain small-particle ZSM-5 zeolites, which were recorded as S-Z5.

1.3 Characterization

The crystal structure of the samples was analyzed by a Rigaku D/Max-3c X-ray diffraction analyzer. The parameters were set as Cu and $K\alpha$ 1 rays, wavelength λ of 0.154 06 nm , room temperature, tube voltage of 40 kV , tube current of 40 mA , 2θ scanning range of $3^\circ\sim 50^\circ$, scanning step of 0.02° , and tracing rate of $0.2\text{ (}^\circ\text{)}\cdot\text{s}^{-1}$.

Cold field emission scanning electron microscopy (SEM), a JEM-2100F field emission transmission electron microscope (TEM), and an Oxford Instruments Limited Oxford/ULTIM MAX instrument were employed to observe the morphologies of the samples. An energy dispersive spectrometer (EDS) was used to analyze the composition of the microregion on the surface of the sample. Before the TEM test, the sample was first ground, dissolved in anhydrous ethanol for ultrasonic dispersion, dropped on a copper net, and then tested after natural air drying at an accelerating voltage of 300 kV.

According to the SEM images, the crystal lengths of the axes a , b , and c of the ZSM-5 zeolites were calculated as L_a , L_b , and L_c (nm), respectively, and the surface area of each crystal face was calculated accordingly. The crystal surface areas $S_{[100]}$, $S_{[010]}$, and $S_{[101]}$ (nm²) of L-Z5, S-Z5, and C-Z5 are calculated as follows^[23]:

$$S_{[100]} = 2 \times L_b \times \left(L_c - 2 \times \frac{L_a}{2 \times \tan(118^\circ/2)} \right) \quad (1)$$

$$S_{[010]} = 2 \times L_a \times \left(L_c - \frac{L_a}{2 \times \tan(118^\circ/2)} \right) \quad (2)$$

$$S_{[101]} = 4 \times L_b \times \frac{L_a}{2 \times \sin(118^\circ/2)} \quad (3)$$

The crystal surface areas $S'_{[100]}$, $S'_{[010]}$, and $S'_{[101]}$ (nm²) of N-ZSM-5 were calculated as follows^[24]:

$$S'_{[100]} = 2 \times L_b \times L_c \quad (4)$$

$$S'_{[010]} = 2 \times L_a \times L_c \quad (5)$$

$$S'_{[101]} = 2 \times L_a \times L_b \quad (6)$$

The exposure ratio $d_{[010]}$ of the [010] crystal plane was calculated by the following formula^[23]:

$$d_{[010]} = \frac{S_{[010]}}{S_{[100]} + S_{[010]} + S_{[101]}} \times 100\% \quad (7)$$

The formula for calculating the proportion of straight channel p_{str} and sinusoidal channel p_{sin} of the zeolite is as follows:

$$p_{\text{str}} = \frac{S_{[010]} \times n_{[010]}}{S_{[100]} \times n_{[100]} + S_{[010]} \times n_{[010]} + S_{[101]} \times n_{[101]}} \times 100\% \quad (8)$$

$$p_{\text{sin}} = (1 - p_{\text{str}}) \times 100\% \quad (9)$$

where, n is the number of holes per unit area of the corresponding crystal face, where $n_{[100]} = 0.748$, $n_{[010]} = 0.743$, and $n_{[101]} = 0.416$.

N_2 adsorption-desorption isotherm and specific surface area: Using N_2 as the adsorption gas, the adsorption-desorption curve of N_2 on the sample surface was determined by the static volume method using an ASAP2020 Version 4.03 physical adsorption instrument (Micromeritics) at -196°C . The BET equation method was used to calculate the specific surface area (S_{BET}), the BJH method was used to calculate the aperture distribution, and the t-plot method was utilized to calculate the specific surface area (S_{Mic}) and micropore volume (V_{Mic}).

The characterization of NH_3 -TPD was carried out on a Chemisorb 2720 multifunctional automatic temperature programmed chemisorbent produced by Micromeritics Company in the United States. A sample of approximately 0.1 g was loaded into a U-shaped quartz tube, the carrier gas was He (25

mL·min⁻¹), and the sample was pretreated at 550°C for 1 h. The temperature was decreased below 50°C and maintained for 30 min. In addition, 10% of the NH_3 -He was absorbed to saturation, and the temperature was increased to 150°C under a He atmosphere and maintained for 30 min to prevent physical adsorption of NH_3 . Finally, the mixture was heated to 700°C at a rate of $10^\circ\text{C}\cdot\text{min}^{-1}$, and the NH_3 -TPD curves were recorded synchronously.

The elemental composition of the product was analyzed by Bruker S8 TIGER X-ray fluorescence spectrometer (XRF). The sample was dried, pressed and scanned. The content of Si-Al oxide in the sample was determined to calculate the Si-Al ratio of the sample.

The ^{27}Al and ^{29}Si MAS NMR of zeolite samples were measured by Agilent 600M nuclear magnetic resonance analyzer with sodium aluminate (NaAlO_2) and tetramethylsilane (TMS) as reference materials, respectively. The Si-Al ratio of the molecular sieve skeleton was obtained by the following formula^[23]:

$$n_{\text{SiO}_2}/n_{\text{Al}_2\text{O}_3} = \frac{\sum_{n=0}^4 I_{\text{Si}(n\text{Al})}}{\sum_{n=0}^4 0.25n[I_{\text{Si}(n\text{Al})}]} \quad (10)$$

where, $I_{\text{Si}(n\text{Al})}$ is the area of the formant corresponding to $\text{Si}(n\text{Al})$, and n is the number of Al atoms in different structures.

1.4 Catalyst performance evaluation and product analysis

Catalyst evaluation: A continuous-flow fixed bed reaction device was used to evaluate catalyst performance, and the evaluation process is shown in Fig. 1. The inner diameter of the reactor was 10 mm, the length was 300 mm, and the three-stage temperature control ensured that the temperature difference of the bed was controlled at $\pm 1^\circ\text{C}$. Before the reaction, the molecular sieve samples were exchanged with NH_4Cl for ammonium (zeolite : solution = 1 : 20, g·mL⁻¹, in which $c(\text{NH}_4\text{Cl}) = 1.0 \text{ mol}\cdot\text{L}^{-1}$) and calcined to obtain an acidic H-type zeolite catalyst. Then, the mixture was pressed, broken, and screened to 20–40 mesh particles of a certain particle size and loaded into the reaction tube. The catalyst was loaded at 1.0 g each time, and the catalyst bed was filled with an equal amount of quartz sand. The reaction mixture was driven into the reactor by an EPP 010S high-pressure infusion pump (Dalian Yilite Analytical Instruments Co. Ltd.). The reaction products were collected by cold trapping, and liquid samples were taken once every 4 h for analysis.

Product analysis: The composition of the product was analyzed by a Thermo Trace 1310 Gas Chromatograph. The chromatographic column used was a TR-Wax capillary column (60 m × 0.32 mm × 1.0 μm) with an FID detector. N_2 was selected as the carrier gas, and the pressure was 0.5 MPa. The injection volume was 1 μL, the shunt ratio was 50 : 1, and the temperature of the injector and detector was set at 180°C . The temperature of the column temperature box was programmed to increase, the initial temperature was 80°C for 2 min, and then the temperature was increased at $10^\circ\text{C}\cdot\text{min}^{-1}$ to 145°C for 10 min.

The quality correction factor was used to quantitatively calculate the product. The reaction performance of the catalysts was evaluated by the conversion rate of the raw materials, the selectivity of the main and byproducts, and the relative content of xylene, as calculated according to formulas (11)–(14).

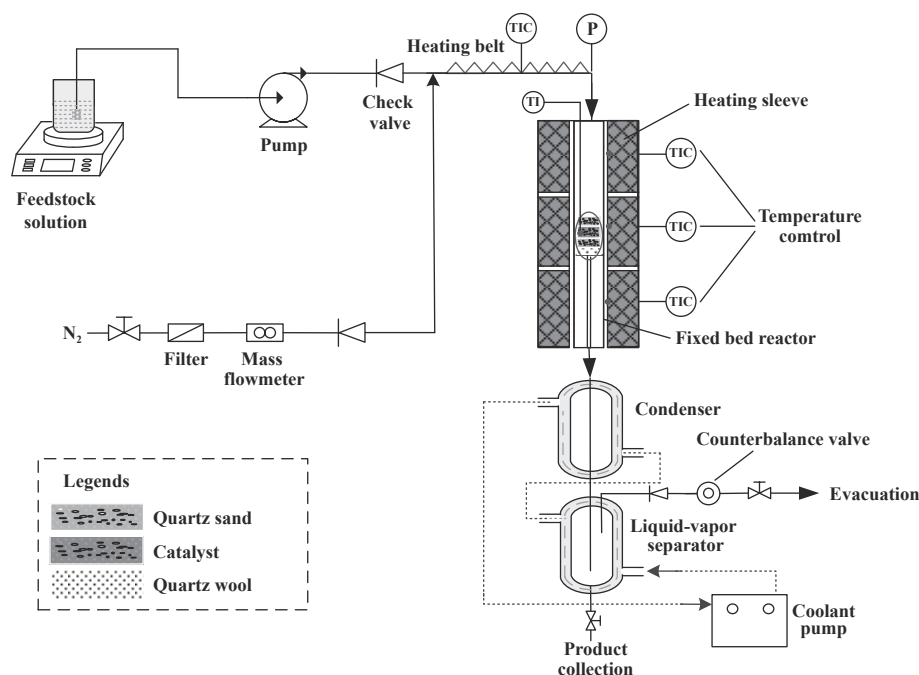


Fig.1 Process diagram of ethanol-benzene alkylation to ethylbenzene

$$X_B = (n_{B,in} - n_{B,out}) / n_{B,in} \times 100\% \quad (11)$$

$$X_E = (n_{E,in} - n_{E,out}) / n_{E,in} \times 100\% \quad (12)$$

$$w_X = m_X / m_{EB} \times 100\% \quad (13)$$

$$S_i = n_i / \sum n_i \times 100\% \quad (14)$$

where X_B and X_E are the conversion rates of the raw material benzene and ethanol, respectively; S_i is the selectivity of product i (toluene, ethylbenzene, propylbenzene, or diethylbenzene). $n_{B,in}$ and $n_{E,in}$ are the amounts of benzene and ethanol in the raw materials, mol, $n_{B,out}$ and $n_{E,out}$ are the amounts of benzene and ethanol in the products, mol, n_i and $\sum n_i$ are the amounts of compound i and all products, mol, m_X and m_{EB} are the masses of xylene and ethylbenzene in the product (g); w_X is the relative content of xylene(%).

2 Results and discussion

2.1 Characterization of ZSM-5

The ZSM-5 zeolite has a typical two-dimensional cross-pore structure. The sinusoidal (or "Z" font) ten-membered ring channel is oriented along the a-axis direction (intersecting the [100] crystal plane), the straight channel is parallel to the b-axis direction (intersecting the [010] crystal plane), and the c-axis direction is the intersection point of the two kinds of channels. The structural characteristics of zeolites determine their acidity, which affects their catalytic activity and selectivity. Differences in the morphology and size of ZSM-5 zeolites affect the length of the two kinds of pore channels, which affects the diffusion behavior of the reactants and catalytic products in the pore channels, thus affecting the catalytic performance of the ZSM-5 catalyst.

Fig. 2 shows the XRD patterns of the zeolite samples. Four types of zeolites exhibited characteristic diffraction peaks with distinct MFI topology at 7.86° , 8.78° , 23.18° , 23.90° , and 24.40° , double peaks at 45.20° , and no diffraction peaks corresponding to other impurities appear, which suggested a

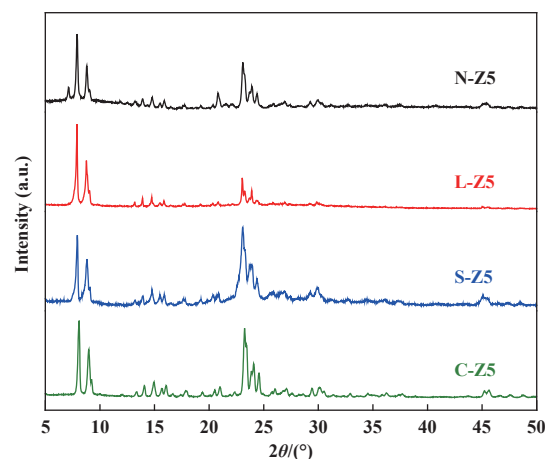


Fig.2 XRD patterns of ZSM-5 zeolites with different morphologies

relatively high crystallinity. In addition, the XRD peaks of L-Z5 were broadened obviously, indicating that its b-axis thickness was small^[25].

Fig. 3 shows SEM images of four kinds ZSM-5 zeolites with different morphologies and sizes. The spheroidal nano-aggregates of the ZSM-5 zeolite samples demonstrated different crystal structures and sizes due to crystal agglomeration, while the crystals of the other three zeolites had regular morphologies and relatively uniform particle sizes. The four zeolites exhibited obvious differences in morphology and size. C-Z5 (Fig. 3(a)) and S-Z5 (Fig. 3(d)) have typical hexagonal prismatic morphologies, but there are certain differences in crystal size. C-Z5 is approximately 1.4 times larger than S-Z5 in the a-axis and c-axis directions, and approximately 1.2 times larger in the b-axis. More importantly, C-Z5 crystals have an obvious cavity structure in the middle (cavity radius between 120 and 160 nm). The crystal sizes S-Z5 and C-Z5 were approximately 380 and 600 nm, respectively. The L-Z5 zeolite with a sheet structure

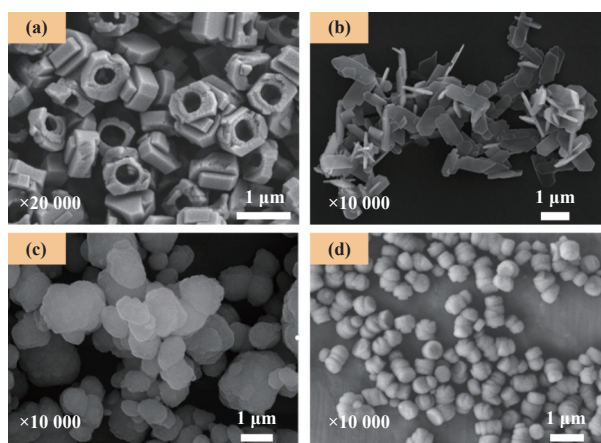


Fig.3 SEM images of ZSM-5 zeolites with different morphologies
(a)C-Z5; (b) L-Z5; (c) N-Z5; (d) S-Z5

was a sheet with a grain length of approximately 1 500 nm, a width of approximately 400 nm, and a thickness of approximately 70 nm (Fig. 3(b)), indicating that a very short b-axis, which was also consistent with the XRD characterization results. As shown in Fig. 3(c), the spheroid N-Z5 zeolite is an approximately spherical aggregate assembled of small particles with a particle size of 50~100 nm, a particle size of approximately 1~1.5 μm , and a rough surface.

Table 1 shows the calculation results of the crystal structure parameters and pore proportions of the four ZSM-5 zeolites with different morphologies and sizes. Among the four zeolites, the L-Z5 zeolites possessed the largest [010] crystal surface area, reaching more than 82%, accompanied by 83.75% of straight pores. The pores of C-Z5 and S-Z5 were relatively small with more than 64% of straight pores, which indicated that molecular diffusion mainly spreads along straight pores in L-Z5, C-Z5, and S-Z5. N-Z5 is quasispherical with three axes located very close to each other, resulting in a significant

Table 1 Crystal parameters of ZSM-5 zeolites with different morphologies and sizes

Sample	Morphology	Crystal parameters			
		Crystal size/nm $L_a \times L_b \times L_c$	[010] exposure degree/%	Straight channel percent/%	Sinusoidal channel percent/%
C-Z5	Cyclic	400×140×600	62.39	68.74	31.26
L-Z5	Lamelliform	400×70×1 500	82.04	83.75	16.25
N-Z5	Spheroid-nanoaggregate	650×550×600	37.49	42.86	57.14
S-Z5	Small particle	300×120×380	56.86	64.60	35.40

reduction in the exposure ratio of the [010] crystal surface area, and the proportion of straight channels is only 42.86%.

Fig. 4 shows the N_2 adsorption-desorption isotherms of zeolites with different morphologies. As shown in Fig. 4(a), the C-Z5, S-Z5, and L-Z5 zeolites exhibited mixed isotherms of I and IV, with adsorption hysteresis loops between the relative pressures $P/P_0=0.4$ and 1.0, indicating a certain degree of mesopores. As shown in Fig. 4(b), the mesopore size of the C-Z5, S-Z5, and L-Z5 zeolites was approximately 3.8 nm (Fig. 4(b)). In contrast to C-Z5, S-Z5, and L-Z5, the N-Z5 prepared by

stepwise crystallization has typical type IV adsorption and desorption isotherms. There are sharp jumps and obvious hysteresis rings in the adsorption-to-desorption isotherms of N-Z5 at higher relative pressures, suggesting a multistage porous zeolite with different mesoporous structures [26]. This observation is also consistent with the electron microscopy results of N-Z5 in Fig. 3(c). Combined with the pore size distribution diagram (Fig. 4(b)) the mesoporous structure of N-Z5 is different in size and disorderly in shape, with relatively wide mesoporous pore size distribution.

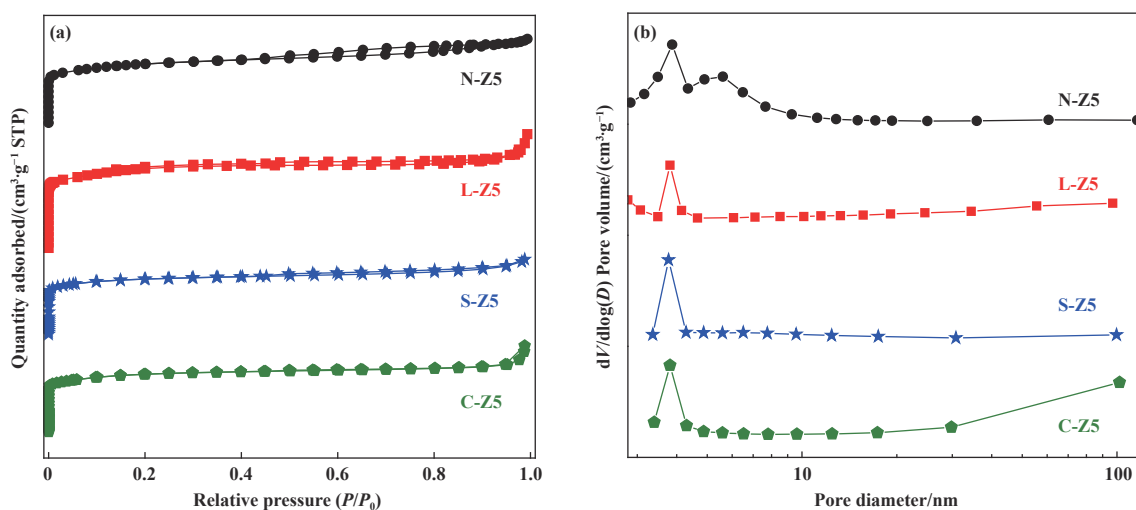


Fig.4 N_2 adsorption-desorption isotherms (a) and BJH pore size distributions (b) of specific surface areas and pore structure data of ZSM-5 zeolites with different morphologies

Table 2 lists the pore structure parameters of zeolites with different morphologies. C-Z5 and S-Z5 had similar pore structure characteristics, as well as similar S_{Ext} , V_{Mic} , and V_{Total} to each other. The micropore volume of the sample is $0.15 \text{ cm}^3 \cdot \text{g}^{-1}$, the external specific surface area is between $46 \sim 48 \text{ m}^2 \cdot \text{g}^{-1}$, and the total pore volume is between $0.22 \sim 0.25 \text{ cm}^3 \cdot \text{g}^{-1}$, indicating that the shell layer of C-Z5 is also highly crystallized. Due to the hollow structure of C-Z5, the specific surface area and micropore area of the C-Z5 zeolite were

slightly greater than those of S-Z5. The specific surface area and pore volume of the N-Z5 samples containing multistage pore structures were significantly greater than those of C-Z5 and S-Z5. Among the four zeolites, the specific surface area and pore volume of thin sheet L-Z5 prepared by adding alcohol were the largest, with S_{BET} and S_{Ext} values up to 595 and $211 \text{ m}^2 \cdot \text{g}^{-1}$, respectively. The highly exposed outer surface of the L-Z5 zeolite had abundant mesoporous structures, which indicated more active sites for alkylation reactions^[27].

Table 2 Specific surface area and pore structure data of ZSM-5 zeolites with different morphologies

Catalyst sample	$S_{\text{BET}} / (\text{m}^2 \cdot \text{g}^{-1})$	$S_{\text{Mic}} / (\text{m}^2 \cdot \text{g}^{-1})$	$S_{\text{Ext}} / (\text{m}^2 \cdot \text{g}^{-1})$	$V_{\text{Total}} / (\text{cm}^3 \cdot \text{g}^{-1})$	$V_{\text{Mic}} / (\text{cm}^3 \cdot \text{g}^{-1})$	$V_{\text{Ext}} / (\text{cm}^3 \cdot \text{g}^{-1})$	Pore size/nm
C-Z5	414	367	47	0.25	0.15	0.10	2.48
L-Z5	595	384	211	0.35	0.16	0.19	2.37
N-Z5	456	295	161	0.27	0.12	0.14	2.58
S-Z5	403	355	48	0.22	0.15	0.08	2.22

S_{BET} : BET surface area; S_{Mic} : Micropore area; S_{Ext} : External surface area; V_{Total} : Total pore volume; V_{Mic} : Micropore volume

The NMR spectra of four ZSM-5 zeolites were showed in Fig. 5. The ^{27}Al NMR spectrum of the sample (Fig. 5(a)), where the formant at the chemical shift $\delta=50$ corresponds to quad-coordination skeleton aluminum, and the formant at $\delta=0$ corresponds to six-coordination non-skeleton aluminum. The four ZSM-5 zeolites all showed strong signal peaks at the chemical shift $\delta=50$, and weak signal peaks at $\delta=0$, indicating that aluminum atoms of the four zeolites mainly exist in the form of tetrad coordination skeleton aluminum. In addition, the

signal peak of C-Z5 sample at $\delta=0$ was the weakest, demonstrated that almost all aluminum atoms entered the hollow ZSM-5 zeolite in the treatment during the crystallization process, which was basically consistent with the characterization results obtained by Qi^[28] who prepared the hollow ZSM-5 zeolite with pure silicon silicalite-1 as the crystal seed. The ^{29}Si NMR spectrum of the sample (Fig. 5(b)) was fitted by peak-differentiation-imitating and obtained four formants. The chemical shift at -107 and -115 were attributed to $Q^1[\text{Si}(0\text{Al})]$,

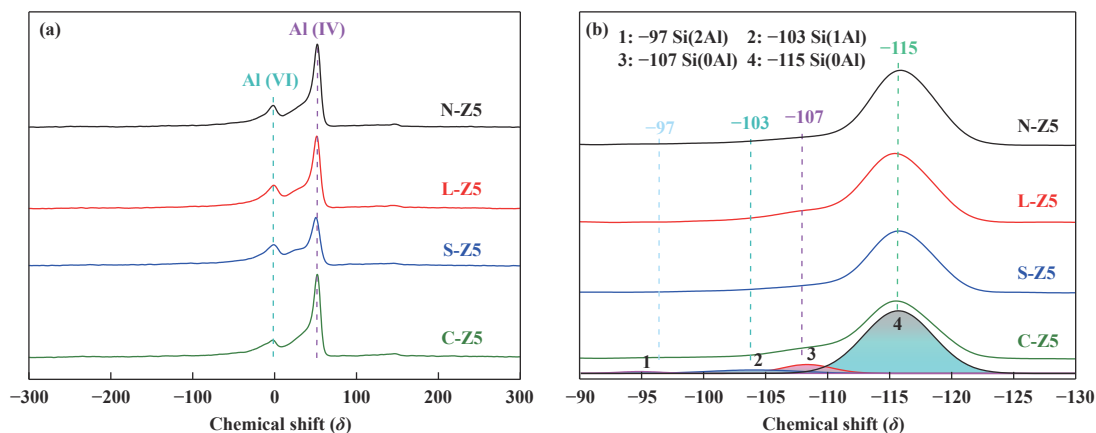


Fig.5 (a) ^{27}Al and (b) ^{29}Si NMR spectra of four ZSM-5 samples

and the chemical shift at -103 were corresponded to $Q^3[\text{Si}(1\text{Al})]$ or the silicon oxygen potential connected to a skeleton aluminum. The fitted peak at -98 corresponded to $Q^2[\text{Si}(2\text{Al})]$ or the silicon bit connecting two skeleton Aluminum^[29]. The Si/Al ratios corresponding to the four samples were calculated, and the results were listed in Table 3. It can be seen that the Si/Al ratio of the four zeolites was close, and was slightly higher than the ratio of feed, indicating that few aluminum atoms entered the ZSM-5 framework, which was consistent with ^{27}Al NMR spectra.

2.2 NH_3 -TPD characterization

Fig. 6 shows the NH_3 -TPD curves of zeolites with different morphologies. The four kinds of zeolites possessed two desorption peaks at 208 and 441 °C, which were attributed to the weak acid and strong acid centers, respectively. The

Table 3 The $n(\text{SiO}_2) : n(\text{Al}_2\text{O}_3)$ of ZSM-5 zeolites with different morphologies

Catalyst sample	$n(\text{SiO}_2) : n(\text{Al}_2\text{O}_3)^a$	$n(\text{SiO}_2) : n(\text{Al}_2\text{O}_3)^b$	$n(\text{SiO}_2) : n(\text{Al}_2\text{O}_3)^c$
C-Z5	60	52	60.5
L-Z5	60	56	61.3
N-Z5	60	55	61.5
S-Z5	60	54	62.8

a. Initial feed ratio;

b. Measured by XRF;

c. Framework silica-to-alumina ratio derived from ^{29}Si NMR spectra.

acidity of the zeolites is closely related to the $\text{SiO}_2 : \text{Al}_2\text{O}_3$ ratio of the zeolite samples. Due to the similar silicon aluminum ratio during the synthesis process, the four kinds of molecular sieves had similar acid strengths. Among them, the S-Z5 zeolite had the strongest high-temperature peak and low-temperature peak. The low-temperature peak (weak acid peak) of the other three zeolites was relatively close, and the strong acid peak was $\text{N-Z5} > \text{C-Z5} > \text{L-Z5}$. The acidity results of the four zeolites were shown in Table 4.

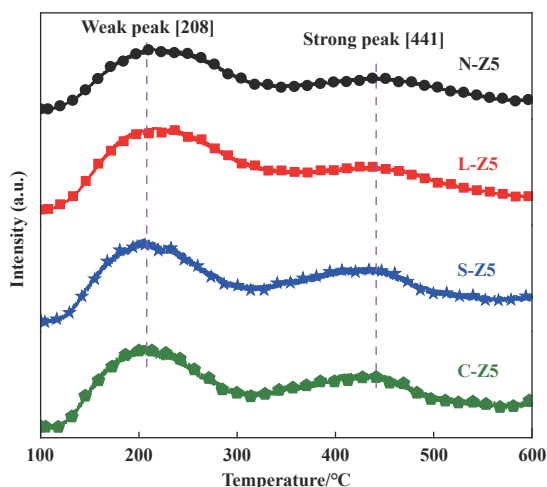


Fig.6 NH_3 -TPD curves of ZSM-5 zeolites with different morphologies

Table 4 Acid properties of ZSM-5 zeolites with different morphologies

Catalyst sample	Acid amount/($\text{mmol} \cdot \text{g}^{-1}$)	
	Weak acid	Strong acid
C-Z5	0.27	0.13
L-Z5	0.25	0.11
N-Z5	0.30	0.14
S-Z5	0.35	0.18

2.3 Catalytic performance of ZSM-5 catalysts

The catalytic alkylation performance of benzene and ethanol by ZSM-5 with different morphologies is listed in Table 3. The conversion rates of four catalysts for ethanol were all above 99.9%, but there is a certain difference in the conversion rate of benzene. As for the conversion rate of benzene, S-Z5 was only 9.45%, and L-Z5 reached 12.48%, which was ascribed to the direct influence of the strong acid peak intensity of the zeolite on the selectivity of ethylbenzene.

There was no significant decrease or deactivation in the reaction after 24 h, but the distribution of alkylation products on four catalysts showed significant differences, as shown in Table 3. For comparison, the data in the table are the average of six experimental results within 24 h of continuous reaction.

Table 5 shows that the ethylbenzene selectivity of the H-ZSM-5 catalysts with different morphologies decreases in the order of L-Z5, C-Z5, N-Z5, and S-Z5 under the same reaction conditions. The ethylbenzene selectivity is not directly related to the acid density or surface area of the zeolite samples. The Si/Al ratios of the four zeolites were similar. The NH_3 -TPD results showed that the weak acid peaks of the four zeolites were similar, but the selectivity of ethylbenzene and the relative content of xylene were very different. Yang *et al.*^[30] studied the use of synthesis gas to produce aromatics and reported that the catalytic performance of zeolites with different Si/Al ratios did not show significant differences, which further indicated that the catalytic performance of different H-ZSM-5 catalysts was also somewhat related to the morphology of the zeolites. In the process of alkylation of benzene and ethanol, raw benzene and the product alkylbenzene (ethylbenzene, diethylbenzene, toluene, and xylene) required different micropore lengths for diffusion in zeolites. Differences in zeolite morphology and grain size inevitably lead to changes in the diffusion paths of reactants and products, thus affecting the selectivity of the products^[19]. Molecular dynamics simulations of the alkylation reaction between benzene and methanol were performed. Yan *et al.*^[16] reported that small molecules diffused along straight and sinusoidal channels, but benzene and alkyl benzene diffused only along straight channels. Table 1 demonstrated that the proportion of straight pores in the thin ZSM-5 zeolite reached 83.75%, with the shortest b-axis length, which was conducive to the diffusion of ethylbenzene and prevented secondary alkylation of ethylbenzene. Moreover, the outer surface of the ZSM-5 zeolite was highly exposed, which promoted benzene and ethanol molecules to contact the acidic sites on the surface. Therefore, the highest selectivity of ethylbenzene was obtained in the alkylation process, reaching 94.56%, and the relative content of xylene was reduced to 0.15% (approximately $1\ 500\ \text{mg} \cdot \text{kg}^{-1}$). The cyclic ZSM-5 zeolite possessed a large cavity structure and relatively thin wall thickness for the rapid diffusion of reaction intermediates, as well as a large number of straight pores for improving the selectivity of ethylbenzene. Compared with straight pores, the proportion of sinusoidal pores in spherical nanoagglomerated ZSM-5 zeolite was larger, and the products diffused along a

Table 5 Results of alkylation of benzene with ethanol on HZSM-5 with different morphologies and sizes

Sample	X_B	X_E	Selectivity/%						
			Ethylbenzene	Diethylbenzene	Toluene	Isopropylbenzene	Propylbenzene	Other	w_X
C-Z5	10.92	99.9	92.25	3.04	1.70	0.75	1.31	0.29	0.71
L-Z5	12.48	99.9	94.56	4.08	0.48	0.45	0.15	0.16	0.15
N-Z5	10.55	99.9	88.60	3.77	2.87	1.57	2.63	0.56	0.93
S-Z5	9.45	99.9	85.86	5.35	3.69	1.63	2.98	0.34	1.03

Reaction conditions: 340 °C, 1.0 MPa, $n(\text{benzene}) : n(\text{ethanol}) = 8 : 1$, $\text{WHSV}(\text{ethanol}) = 1\ \text{h}^{-1}$; X_B : Conversion of benzene/%;

X_E : Conversion of ethanol/%; w_X : Mass fractions of xylene relative to ethylbenzene/%.

zigzag path in the sinusoidal pores, which led to a low diffusion efficiency theoretically. However, the selectivity of ethylbenzene was greater than that of small-grain ZSM-5 zeolite, which has more straight pores but a smaller external specific area. The surface area is large, and the surface is enriched with multistage pores. Notably, this did not indicate that the influence of the external specific area was greater than the influence of the direct channel. As shown in Table 2, the outer area of annular hollow ZSM-5 was smaller than that of small-grain ZSM-5 and much smaller than that of nanospherical ZSM-5, but its catalytic performance was greater than that of nanospherical ZSM-5, which was due to its unique hollow structure. The existence of an annular hollow structure in ZSM-5 resulted in a molecular sieve with nanoscale structural characteristics, multistage pores, and short b-axis ZSM-5, thus greatly improving its catalytic performance.

3 Conclusions

In this paper, four ZSM-5 zeolites with different morphologies and sizes were prepared by the hydrothermal method. The structural differences of the four zeolites were compared, and the effects of their morphologies and sizes on the performance of benzene and ethanol alkylation reactions were explored. The main conclusions were as follows:

The morphology and size of zeolite particles significantly affected the acidity and alkylation properties of zeolites. The weak acid peaks of the four zeolites were close to each other, but the existence of short B-axes and hollow structures decreased the strength of the molecular sieves, which directly affected the selectivity of ethylbenzene.

The morphology and size of zeolite particles affected the pore structure of zeolites. The shorter the b-axis is, the larger the proportion of straight pores in the molecular sieve. The specific surface area, empty volume, and proportion of straight pores in the HZSM-5 zeolites affected the alkylation performance to a certain extent. The influence of four morphologies on the catalytic alkylation performance of benzene and ethanol decreased in the order of sheet ZSM-5, annular ZSM-5, spheroidal nanoagglomerates ZSM-5, and small-grain ZSM-5.

Lower acid strength, larger specific surface area and pore volume, and straighter pore proportion improved the alkylation performance of zeolites, thus enhancing the selectivity of ethylbenzene product.

References

- [1] Sun H M. Ethylbenzene production technology and market analysis[J]. *Technol Ecol Petrochem*, 2019, **35**(5): 18–23.
- [2] Ge H Q, Yin W C, Yang G Q, et al. Review on vanadium oxide catalysts for oxidative dehydrogenation of ethylbenzene with CO₂[J]. *Chem Ind Eng Prog*, 2021, **40**(4): 1868–1882.
- [3] Yang Y X, Deng Y Q. Commercial application of gas-phase alkylation technology SGBE for dry gas to ethylbenzene[J]. *Petrol Process Petrochem*, 2021, **52**(11): 38–41.
- [4] Yang W M, Wang Z D, Sun H M, et al. Advances in development and industrial applications of ethylbenzene processes[J]. *Chin J Catal*, 2016, **37**(1): 16–26.
- [5] Ye L Y. The latest achievements of coal-based ethanol catalysts[J]. *Nat Gas Chem Ind*, 2018, **43**(4): 126–132.
- [6] Zhao Y J, Zhang X, Zhou C L, et al. New synthesis technology of ethyl benzene — Ethyl alcohol to ethyl benzene process technology[J]. *Contemp Chem Ind*, 2011, **40**(11): 1149–1151.
- [7] Pan L R, Li H X. A study of surface acidity and activity and selectivity for alkylation benzene with ethanol of HZSM-5 modified base-earth metal oxides[J]. *Chem J Chin Univ*, 1990, **11**(6): 617–621.
- [8] He J, Sun H M, Huan M Y, et al. Research on liquid phase transalkylation reaction in ethyl benzene production process with benzene [J]. *Adv Fine Petrochem*, 2011, **12**(2): 39–42.
- [9] Dong Z W, Yang C Y, Zhao D P, et al. Co-crystalline ZSM-5/ZSM-11 nanostructures for alkylation of benzene with ethanol[J]. *ACS Appl Nano Mater*, 2021, **4**(10): 10296–10306.
- [10] Odedairo T, Al-Khattaf S. Ethylation of benzene: Effect of zeolite acidity and structure[J]. *Appl Catal A-Gen*, 2010, **385**(1/2): 31–45.
- [11] Corma A, Llopis F J, Martínez C, et al. The benefit of multipore zeolites: Catalytic behaviour of zeolites with intersecting channels of different sizes for alkylation reactions[J]. *J Catal*, 2009, **268**(1): 9–17.
- [12] Sridevi U, Bokade V V, Satyanarayana C V V, et al. Kinetics of propylation of benzene over H-Beta and SAPO-5 catalysts: A comparison[J]. *J Mol Catal A-Chem*, 2002, **181**(1): 257–262.
- [13] Corma, A, Martínez-Soria V, Schnoefeld, E. Alkylation of benzene with short-chain olefins over MCM-22 zeolite: Catalytic behaviour and kinetic mechanism[J]. *J Catal*, 2000, **192**(1): 163–173.
- [14] Odedairo T, Al-Khattaf S. Comparative study of zeolite catalyzed alkylation of benzene with alcohols of different chain length: H-ZSM-5 versus mordenite[J]. *Catal Today*, 2013, **204**: 73–84.
- [15] Zhang Y F, Zhu P, Zhang X F, et al. Alkylation of benzene with ethanol to ethylbenzene over bowl-like hollow ZSM-5 zeolite catalysts[J]. *Mod Chem Ind*, 2023, **43**(1): 185–191+197.
- [16] Yan Z G, Chen D, Huang L, et al. A theoretical insight into diffusion mechanism of benzene-methanol alkylation reaction in ZSM-5 zeolite[J]. *Microporous Mesoporous Mater*, 2022, **337**: 111926.
- [17] Huang S Y, Ren Y H, Huang S S, et al. Synthesis of ZSM-5 zeolite with different morphologies and catalytic performance of methanol to gasoline[J]. *J Guangxi Univ(Nat Sci Ed)*, 2020, **45**(2): 414–420.
- [18] a. Zheng B M, Fang X C, Guo R, et al. Hierarchical ZSM-5 zeolite: Synthesis and application in oil refinery[J]. *J Mol Catal (China)*, 2017, **31**(5): 486–500.
b. Liao Z K, Dilinuer A, Fang Y P, et al. Effect of K⁺ modified Au/ZSM-5 zeolite catalyst on cracking performance of n-butane. *J Mol Catal (China)*, 2023, **37**(2): 118–129.
c. Zhu W S, Yang S C, Xue X X, et al. Preparation of BiZrO₃/ZSM-5 catalyst for direct aromatization of syngas. *J Mol Catal (China)*, 2022, **36**(1): 32–41.
d. Li B Z, Wang K L, Li Y X. Study on NH₃-SCR reaction mechanism over MnZSM-5 catalyst. *J Mol Catal (China)*, 2022, **36**(4): 313–320.
- [19] Li G X, Zhang Y F, Dong P, et al. Research progress of ZSM-5 molecular sieve catalyzing alkylation of benzene with methanol[J]. *J Mol Catal (China)*, 2019, **33**(6): 570–577.
- [20] Zhu P, Wang J S, Xia F, et al. Alcohol-assisted synthesis of sheet-like ZSM-5 zeolites with controllable aspect ratios[J]. *Eur J Inorg Chem*, 2023, **26**(9): e202200664.
- [21] Zhang L, Xia F, Li X X, et al. Synthesis and characterization of cyclic ZSM-5 zeolites[J]. *Petrochem Technol*, 2023, **52**(7): 895–902.
- [22] Wang Y, Li S, Liu Y C, et al. Hierarchical ZSM-5 zeolite fabricated with loosely nanocrystallite aggregates without secondary template[J]. *Ind Eng Chem Res*, 2022, **61**(25): 9136–9148.
- [23] Liu X L, Shi J, Yang G, et al. A diffusion anisotropy descriptor links morphology effects of H-ZSM-5 zeolites to their catalytic cracking performance[J]. *Commun Chem*, 2021, **4**(1): 107.
- [24] Li W Q, Li Y F, Liu B, et al. Effect of morphology and size of ZSM-5 zeolites on catalytic cracking of hexene to propylene[J]. *Nat Gas Chem Ind*, 2022, **47**(4): 113–119.
- [25] Zhang S Y, Tao J Q, Shen Y, et al. Low cost synthesis and catalytic cracking performance of ZSM-5 zeolites[J]. *Petrochem Technol*, 2022, **51**(9): 1017–1025.
- [26] Sun L L, Yan K, Luo W, et al. Hollow ZSM-5 zeolite microspheres with improved adsorption and catalytic properties[J]. *J Inorg Mater*, 2016, **31**(8): 834–840.
- [27] Zhou A J, Zhang J X, Yang H, et al. Synergetic and efficient alkylation of benzene with ethane over Pt/ZSM-5 nanosheet bifunctional catalysts to ethylbenzene[J]. *Fuel*, 2023, **342**: 127764.
- [28] Qi Z F, Zhuo Z X, Hu C H, et al. Synthesis of hollow structured ZSM-5 using silicalite1 as seeds[J]. *J Mol Catal (China)*, 2021, **35**(6): 495–502.

- [29] Wang S, Wang P F, Qin Z F, *et al.* Relation of catalytic performance to the aluminum siting of acidic zeolites in the conversion of methanol to olefins, viewed *via* a comparison between ZSM-5 and ZSM-11[J]. *ACS Catal*, 2018, 8(6): 5485–5505.
- [30] Yang J H, Pan X L, Jiao F, *et al.* Direct conversion of syngas to aromatics[J]. *Chem Commun*, 2017, 53(81): 11146–11149.

ZSM-5 分子筛形貌对苯-乙醇烷基化催化性能的调控作用

张亮, 夏飞, 袁亚飞, 李啸贤, 郭淑静, 张伟*

(陕西延长石油(集团)有限责任公司大连化物所西安洁净能源(化工)研究院, 陕西 西安 710075)

摘要: 采用水热法制备了环状、薄片、类球状聚集体和小晶粒 4 种不同形貌和尺寸的纳米 ZSM-5 分子筛, 用 XRD、SEM、BET、MAS-NMR 和 NH₃-TPD 对所合成分子筛进行了表征, 并考察分子筛形貌对苯和乙醇烷基化性能的影响. 实验结果表明: 在相近的硅铝比下, 不同形貌的分子筛具有相似的弱酸峰强度, 短 b 轴和中空结构的存在会降低分子筛的强酸峰强度, 分子筛的强酸峰强度直接影响烷基化性能; 分子筛颗粒形貌对催化烷基化性能有较大影响, 4 种形貌分子筛催化苯和乙醇烷基化性能优劣顺序为: 薄片 ZSM-5>环状 ZSM-5>类球状团聚体 ZSM-5>小晶粒 ZSM-5. 其中, 具有薄片结构的 H-ZSM-5 分子筛在烷基化反应过程中表现出相对较好的催化性能. 综合对比结果表明: 较低的强酸强度、较大的比表面积和孔容、较多的直形孔道占比下, 分子筛的烷基化性能较好, 产物乙苯的选择性越高.

关键词: ZSM-5 分子筛; 合成; 形貌; 催化性能